Integrated Control of Steering and Braking for Path Tracking using Multi-Point Linearized MPC

Jonghyup Lee, Seibum B. Choi

***Abstract*—In this study, we propose an integrated braking and steering model predictive controller for stable and accurate path tracking. To perform model-based longitudinal control and lateral control at the same time, it is necessary to consider nonlinear characteristics caused by changing vehicle speed and nonlinear tire forces. This paper proposes a multipoint linearization method to minimize the linearization error, and a controller with good computational efficiency and accurate consideration of nonlinear vehicle behavior is also introduced. In addition, the proposed model predictive controller (MPC) actively utilizes the road friction limit constraint for each tire force to ensure vehicle stability. Through this, the proposed controller generates optimal braking and steering inputs for situations such as high-speed turns in which braking must be involved. Due to the proposed linearized model, the controller achieves a significant improvement in computational efficiency and good control performance similar to that of the nonlinear MPC. Comparison with other control methods and performance verification for various road conditions are performed through simulations, and the results show very efficient calculation while performing accurate path tracking.**

***Index Terms*—Control and Optimization, Vehicle control; Driver assistance, Control of dynamic systems**

I. Introduction

OVER the past several decades, vehicle safety has become one of the biggest vehicle performance indicators, and all vehicle manufacturers have conducted research and development in various area to increase vehicle safety. Vehicle chassis control has contributed greatly to improving vehicle safety performance, sharply reducing the accident rate by securing vehicle driving stability. As the development of intelligent vehicles has accelerated, technology such as cameras and radar sensors for recognizing conditions around vehicles has greatly developed. These technologies enable vehicle controls that increase safety against dangerous surrounding situations. The advanced driver assistance system (ADAS), based on recognition information such as that from autonomous emergency braking (AEB) and emergency lane keeping (ELK) systems, has proven its excellent accident prevention performance [1]–[5].

Path tracking control is a type of vehicle position control that follows the desired path created from a path planner that plans a future path for various purposes [6]–[10]. Path tracking control is achieved through turning control and speed control, and it is essential for lane keeping/changing and obstacle avoidance behavior. Due to the importance of path tracking control, numerous control methods such as model free control [11], kinematic model based control [12]–[14], dynamic model based control without prediction and model predictive control (MPC) [7], [15]–[26] have been introduced [15], [16]. In particular, path tracking control using MPC can consider the physical limitations of inputs and outputs, and it becomes possible to calculate the optimal input through future prediction. Therefore, this method is discussed as the most suitable method for path tracking control.

MPC is divided into linear MPC (LMPC) and nonlinear MPC (NMPC) according to the characteristics of the model used [27], [28]. Because the dynamic model used for path tracking control is non-linear, studies using NMPC have been introduced [17], [18]. Path tracking control with NMPC works by solving a constrained nonlinear optimization problem. However, since the nonlinear optimization such a requires great computational effort, it has a limitations in real-time implementation. Some studies have attempted to solve this problem by linearizing nonlinear dynamic models.

Compared to NMPC, LMPC using a linearized model has the advantage of significantly reducing the amount of computational effort by utilizing linear optimization such as quadratic programming [19]–[22]. The linearized model, by using a Taylor expansion, can be a good replacement model for the nonlinear model if the states are close to the linearization points. However, this approach also has the disadvantage that the model accuracy decreases as the prediction state moves away from the linearization point during the prediction horizon. This reduction in model accuracy impairs the prediction accuracy of the model predictive controller, and can be a major cause of control performance degradation, resulting in path tracking error and excessive slip in dangerous situations. In particular, performance can be further degraded when longitudinal control is also implemented, as the nonlinearity of the vehicle model increases as the speed changes.

In this study, we propose a novel type of LMPC for path tracking using the multi-point linearized model to solve the aforementioned problems. MPC makes predictions at every step about the states and inputs during the prediction horizon. The strong point of the proposed linearized model is that it requires the same level of computation as the existing linear model, while maximally reflecting the nonlinearity of the model. Therefore, using the proposed linear model, the proposed controller is efficiently calculated while sufficiently reflecting the nonlinear behavior.

In addition, as the efficient use of nonlinear models becomes possible, we propose in this study a controller based on the nonlinear tire force constraint. When the force of a single tire

Jonghyup Lee and Seibum Choi (Corresponding author) are with the Korea Advanced Institute of Science and Technology (KAIST), 291, Daehak-ro Yuseong-gu, Daejeon, 34141, South Korea
(e-mail: jonghyuplee@kaist.ac.kr;sbchoi@kaist.ac.kr).

exceeds the road friction limit, the vehicle rapidly becomes unstable. Therefore, existing macro-constraints such as lateral acceleration and lateral slip angle [7], [17] can indirectly secure vehicle safety, but cannot guarantee that all tires remains in stable slip region. In other words, even if constraints such as acceleration are satisfied, the vehicle may become unstable due to excessive slip. In this study, the safety of the vehicle is more accurately secured through the constraint that the sum of the longitudinal and lateral forces of each wheel does not exceed the road friction limit. Because, in contrast to the conventional model, this requires calculation of the tire force, the use of a large non-linear constraint is inevitable, however, this constraint can be efficiently calculated through the proposed linearization method. Through this, the proposed controller automatically generates a braking input for stable operation even in high-speed situations without a separate longitudinal speed planner; system generates a steering input that accurately follows the desired path. This produces minimal braking for a stable turn, as braking input is applied only when the tire force constraint is expected to be violated. In addition, depending on the situation, the maximum tire force can be used to cope with as many dangerous situations as possible.

The main contributions of this paper are: 1) A multi-point linearization model using predicted states and inputs is proposed to linearize the nonlinear model used in the controller with minimal error. 2) Through the design of the LMPC using the integrated prediction model and tire force constraints, a path tracking controller that can accurately and safely cope with high-speed situations was proposed. Finally, improved calculation speed and stable control performance of the proposed controller compared to NMPC are confirmed.

The remainder of this paper is organized as follows: In section II, the nonlinear vehicle model including the vehicle dynamics model, tire model, and relative position model are presented. In section III, an LMPC based path tracking controller that uses a multi-point linearized vehicle model is proposed. Sections IV verifies through simulation analysis the control performance of the proposed path tracking controller. Conclusion is provided in section V.

II. Nonlinear Vehicle Model

This section introduces a vehicle model that will be used to predict vehicle behavior. Since the controller proposed in this study is a model-based controller using a mathematically expressed vehicle motion model, it is necessary to establish an accurate system equation. For the design of the integrated controller, the vehicle model used in this study simultaneously addresses the longitudinal and lateral behavior of the vehicle. To consider the relationship between the tire force of each wheel and the road surface friction limit, the longitudinal, lateral, and vertical forces of each tire were modeled. In addition, a relative position model expressing relative position and angle relative to path is used to predict tracking errors.

A. Planar Vehicle Model

The planar vehicle model shown in Fig.1 is a vehicle model that can handle longitudinal, lateral, and yaw motion of the vehicle. The model is expressed through force balance equations and the yaw moment balance equation. The three velocity states of the vehicle, longitudinal velocity v_x, side slip angle β and yaw rate $\dot{\psi}$, are described by the following equations [29], [30]:

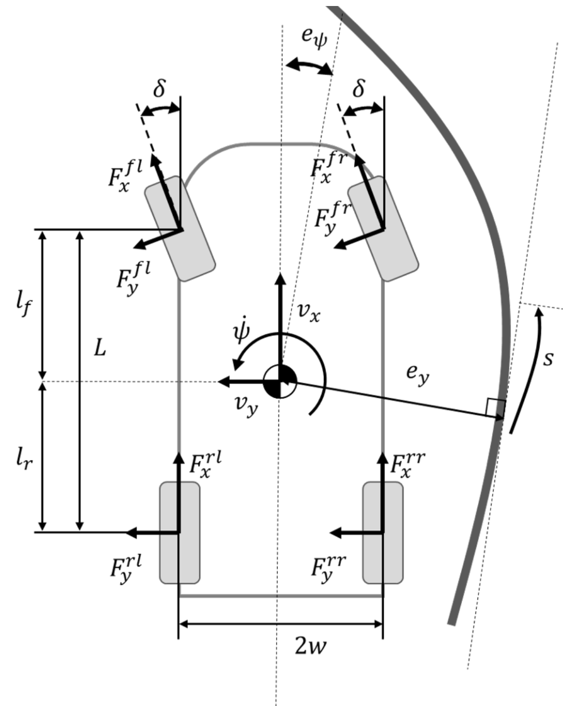

Fig. 1. The planar vehicle model and the relative position model

$$
\begin{aligned}
\dot{v_x} =& \frac{1}{m}[\left(F_x^{fl}+F_x^{fr}\right)\cos\delta \ + F_x^{rl}+F_x^{rr} \\
&-\left(F_y^{fl}+F_y^{fr}\right)\sin\delta \ - F_D] + v_x\beta\dot{\psi}, && (1)\\
\dot{\beta} =& \frac{1}{mv_x}[\left(F_x^{fl}+F_x^{fr}\right)\sin\delta \ + \left(F_y^{fl}+F_y^{fr}\right)\cos\delta \\
&+F_y^{rl}+F_y^{rr}] - \dot{\psi}, && (2)\\
I_z\ddot{\psi} =& l_f[\left(F_y^{fl}+F_y^{fr}\right)\cos\delta + \left(F_x^{fl}+F_x^{fr}\right)\sin\delta] \\
&- l_r\left(F_y^{rl}+F_y^{rr}\right) + w[(F_y^{fl}-F_y^{fr})\sin\delta \\
&+(F_x^{fr}-F_x^{fl})\cos\delta \ + (F_x^{rr}-F_x^{rl})], && (3)
\end{aligned}
$$

where F_x, F_y, F_D, δ, m, I_z, l_f, l_r, and w are the longitudinal tire force, lateral tire force, air drag force, wheel steering angle, vehicle mass, vehicle moment of yaw inertia, distance from front axle to vehicle center of gravity (CG), distance from rear axle to the vehicle CG, and half of track width, respectively. The superscripts fl, fr, rl, and rr represent the front left, front right, rear left, and rear right wheels.

B. Tire Forces Calculation

The tire forces of each wheel required to calculate the vehicle motion in the planar vehicle model and to consider the road surface friction limit are modeled and calculated for the longitudinal, lateral, and vertical directions.

Assuming that the braking torques of the left and right wheels are the same and that the wheel inertia can be neglected, it can be assumed that the left and right braking forces are identical. Then, from the Equation (1), the braking force of each wheel is expressed as follows [31].

$$\begin{aligned} F_x^{fl} = F_x^{fr} =& \frac{\lambda}{2\left[1-\lambda\left(1-\cos\delta\ \right)\right]} \\ & \left[ma_x + \left(F_y^{fl}+F_y^{fr}\right)\sin\delta\ + F_D\right], \\ F_x^{rl} = F_x^{rr} =& \frac{(1-\lambda)}{2\left[1-\lambda\left(1-\cos\delta\ \right)\right]} \\ & \left[ma_x + \left(F_y^{fl}+F_y^{fr}\right)\sin\delta\ + F_D\right], \end{aligned} \tag{4}$$

where a_x and λ denote the longitudinal acceleration and the braking ratio of the front and rear axles, respectively, with a small steering angle assumption, ($\delta \ll 1$), these can be simplified.

$$\begin{aligned} F_x^{fl} = F_x^{fr} &= \frac{\lambda}{2}\left[ma_x + \left(F_y^{fl}+F_y^{fr}\right)\delta + F_D\right], \\ F_x^{rl} = F_x^{rr} &= \frac{(1-\lambda)}{2}\left[ma_x + \left(F_y^{fl}+F_y^{fr}\right)\delta + F_D\right]. \end{aligned} \tag{5}$$

Using the brushed tire model, the lateral tire force can be modeled as follows [32], [33].

$$\begin{aligned} F_y^i =& C_\alpha(\alpha) \\ =& \begin{cases} C_0\tan\left(\alpha^j\right)\ - \frac{C_0^2}{3\mu F_z^j}\left|\tan\left(\alpha^j\right)\ \right|\tan\left(\alpha^j\right) \\ +\frac{C_0^3}{27\mu^2 F_{z,i}^2}\tan^3\left(\alpha^j\right)\ , \text{if}\left|\alpha^j\right| < \tan^{-1}\left(\frac{3\mu F_z^j}{C_0}\right) \\ \mu F_z^j sgn\left(\alpha^j\right)\ , \text{if}\left|\alpha^j\right| > \tan^{-1}\left(\frac{3\mu F_z^j}{C_0}\right), \end{cases} \end{aligned} \tag{6}$$

where C_α is the cornering stiffness with respect to the slip angle α, C_0 is the cornering stiffness at the linear region(i.e.$|\alpha^j| \ll 1$), μ denotes the road friction coefficient, and F_z^j is the vertical force of each tire. The tire slip angle α^j can be expressed as :

$$\alpha^j = \tan^{-1}\frac{v_{ty}^j}{v_{tx}^j}, \tag{7}$$

where,

$$\begin{aligned} v_{tx}^j &= \begin{cases} -v_{w,x}^j\sin\delta + v_{w,y}^j\cos\delta \\ -v_{w,x}^j & , j = fl, fr \end{cases} \\ v_{ty}^j &= \begin{cases} v_{w,x}^j\cos\delta + v_{w,y}^j\sin\delta \\ v_{w,y}^j & , j = rl, rr, \end{cases} \end{aligned} \tag{8}$$

longitudinal velocity $v_{w,x}^j$ and lateral velocity $v_{w,y}^j$ of each wheel position can be calculated from the vehicle velocity, side slip angle, and yaw rate.

The maximum forces that each tire can generate are proportional to the vertical force. Therefore, the vertical force of each wheel needs to be accurately calculated not only to determine the lateral tire force in Equation (6), but also to consider the road surface limit. Load transfer occurs due to the vehicle's longitudinal and lateral acceleration. The load transfer amount is proportional to the magnitude of the acceleration and is determined by the shape of the vehicle and the rigidity of the suspension [29]. In particular, because the front/rear roll stiffnesses of the vehicle are different, the front/rear roll stiffness ratio is dominant in the case of lateral load transfer. The normal force of each wheel F_z^j can be calculated as:

$$\begin{aligned} F_z^{fl} &= \frac{l_r}{2L}mg - \frac{h_{cg}}{2L}ma_x + \sigma_f ma_y, \\ F_z^{fr} &= \frac{l_r}{2L}mg - \frac{h_{cg}}{2L}ma_x - \sigma_f ma_y, \\ F_z^{rl} &= \frac{l_f}{2L}mg + \frac{h_{cg}}{2L}ma_x + \sigma_r ma_y, \\ F_z^{rr} &= \frac{l_f}{2L}mg + \frac{h_{cg}}{2L}ma_x - \sigma_r ma_y, \end{aligned} \tag{9}$$

where a_y, g, L, and h_{cg} are lateral acceleration, gravitational acceleration, distance from front axle to rear axle, and height of vehicle CG. The lateral load transfer coefficients σ_f and σ_r are calculated from the simplified roll dynamics model shown in Fig.2, as follows.

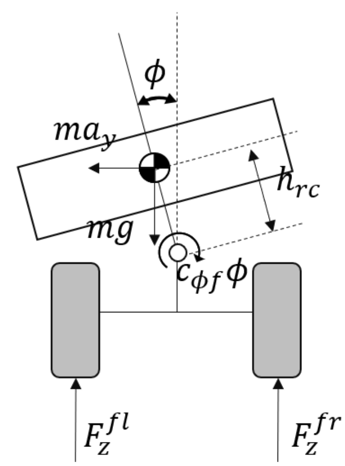

Fig. 2. Simplified roll dynamics model

$$\begin{aligned} \sigma_f &= \frac{1}{w}\left(\frac{c_{\phi f}h_{rc}}{c_{\phi f}+c_{\phi r}-mgh_{rc}} + \frac{l_r}{L}(h_{cg}-h_{rc})\right), \\ \sigma_r &= \frac{1}{w}\left(\frac{c_{\phi r}h_{rc}}{c_{\phi f}+c_{\phi r}-mgh_{rc}} + \frac{l_f}{L}(h_{cg}-h_{rc})\right), \end{aligned} \tag{10}$$

where $c_{\phi f}$, $c_{\phi r}$, and h_{rc} are the front roll stiffness, rear roll stiffness, and distance from CG to roll center.

C. Relative Position Model

The relative position model describing changes in the relative position and relative angle with respect to the desired path, is constructed by expressing the station(longitudinal position on path) s, the lateral distance error e_y, and the heading angle error e_ψ as shown in Fig.1 [23]:

$$\dot{s} = v_x\left(\cos e_\psi - \beta\sin e_\psi\right), \tag{11}$$

$$\dot{e_y} = v_x\left(\sin e_\psi - \beta\cos e_\psi\right), \tag{12}$$

$$\dot{e_\psi} = \dot{\psi} - \kappa(s)\dot{s}, \tag{13}$$

where κ is the curvature of the desired path, expressed as a function for station s by utilizing the information on the desired path.

D. Integrated Nonlinear Vehicle Model

Finally, the total state vector is created by integrating the velocity states $[v_x, \beta, \dot{\psi}]^T$ expressed through (1)-(3) and the displacement states $[s, e_y, e_\psi]^T$ expressed through (11)-(13); due to the time-varying variable κ, the state function is a time-varying function. By integrating and discretizing Equations (1)-(13), the integrated nonlinear vehicle model can be expressed.

$$x(k+1) = f_k\left(x(k), u(k)\right), \tag{14}$$

where, $x = [v_x, \beta, \dot{\psi}, s, e_y, e_\psi]^T, \quad u = [\delta, a_x]^T$.

III. Controller design

In this section, we introduce the model predictive controller and the state prediction model. In particular, the multi-point linearization method, which minimizes the linearization error, is proposed. In addition, the process of converting a nonlinear optimization problem into a linear optimization problem using a multi-point linearized model is described in detail.

The general structure of the nonlinear model predictive controller is as follows [27].

$$\begin{aligned} &\arg\min_{U_k} J\left(x(k), U_k\right), \\ &\underset{i=0,1,\dots,N-1}{\text{subject to.}} \quad x_{0|k} = x(k), \\ &\qquad x_{i+1|k} = f_k(x_{i|k}, u_{i|k}), \\ &\qquad x_{i+1|k} \in X_k \subset \bar{X}_k, \\ &\qquad u_{i|k} \in U_k \subset \bar{U_k}, \\ &\qquad u(k) = u_{0|k}, \end{aligned} \tag{15}$$

where, J is a cost function designed for the purpose of controller. $x_{i|k}$, $u_{i|k}$, and N are the predicted states after i steps predicted at the k-th step, the planned inputs after i steps calculated in the k-th step, and the number of prediction steps. Specifically, $x_{0|k}$, which is the initial value for the prediction, is determined by measuring or estimating the states at the current step. The state sequence and the control sequence, X_k and U_k are as follows.

$$X_k = \begin{bmatrix} x_{1|k} \\ x_{2|k} \\ x_{3|k} \\ \vdots \\ x_{N|k} \end{bmatrix}, U_k = \begin{bmatrix} u_{0|k} \\ u_{1|k} \\ u_{2|k} \\ \vdots \\ u_{N-1|k} \end{bmatrix}.$$

$\bar{X}_k$ and $\bar{U}_k$ are the constrained sets of the state sequence and the control sequence respectively. The control sequence U_k obtained through optimization minimizes the cost function while satisfying the constraints. Only the first element is applied to the plant in the MPC framework. By defining an appropriate cost function and constraint, we realize the final goal of this study, a stable and accurate path tracking controller. And these are introduced in detail in III-B.

A. Multi-Point Linearized Prediction Model

In the MPC framework (15), MPC generates a control input through optimization based on the relationship between the input sequence U_k and the state sequence X_k. Therefore, model prediction control is greatly influenced by the prediction accuracy. This means that if, to reduce the computational burden, the prediction performance of the linearized model is significantly reduced compared to that of the original nonlinear model, the expected control performance cannot be achieved.

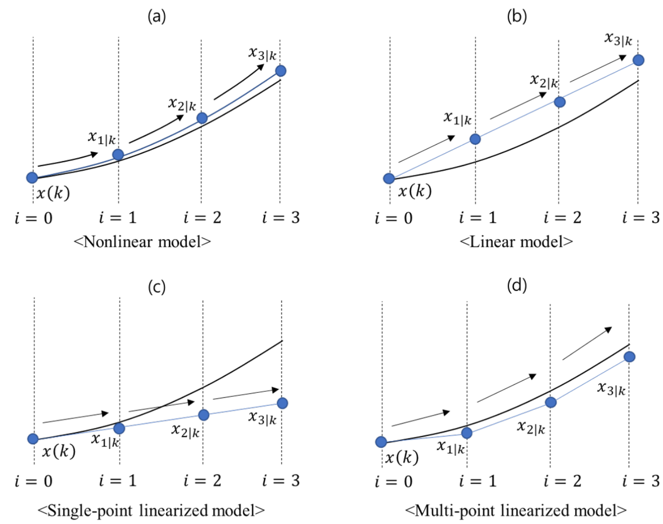

Fig. 3. Conceptual diagrams of prediction methods

Fig.3 is the conceptual diagram of a predictive model designed based on various system models. Fig. 3(a) shows the concept of the predictive model using the original non-linear model [17], [18]; Fig.3(b) shows a case in which a linear model with appropriate assumptions, such as the linear bicycle model, is used [7]. And, Fig.3(c) and Fig.3(d) show prediction methods using a single-point linearized model [20], [21] and a multi-point linearized model, respectively. Prediction using a nonlinear model for a nonlinear system has accurate prediction performance; however, if a linear model is used as in Fig.3(b) or Fig.3(c), accurate prediction cannot be expected. In particular, in the case of single-point linearization, no matter how logically the linearization points are selected, the prediction errors accumulate as the predicted states and inputs move away from them. Therefore, prediction accuracy is poor for systems with strong nonlinearity or long prediction horizon.

In [22], effective linear time varying (LTV) model was used through multi-point linearization for the predicted future states using integration with respect to the previous input $u(k-1)$. However, this method is also difficult to reflect the input change during prediction, and the prediction accuracy is inevitably lowered. In this study, multi-point linearization is performed based on the state sequence X_{k-1} and input sequence U_{k-1} calculated in the previous step. During the prediction horizon, states and inputs behave similarly to the predictions of the previous step. Compared to the method in [22], the proposed method can minimize the linearization error even for changes in the future input by considering the predicted future inputs during the prediction horizon. Therefore, the proposed model can represent the nonlinear model with higher accuracy than the above-mentioned models, and high prediction accuracy can be expected.

The multi-point linearization of the nonlinear vehicle model (14) for the state sequence X_{k-1} and input sequence U_{k-1}, predicted in the previous step, is expressed as:

$$
\begin{aligned}
&x_{i+1|k} \\
&\quad = f_k(x_{i+1|k-1}, u_{i+1|k-1}) \\
&\qquad + \nabla_x f_k(x,u)|^{x_{i+1|k-1}}_{u_{i+1|k-1}}(x_{i|k} - x_{i+1|k-1}) \\
&\qquad + \nabla_u f_k(x,u)|^{x_{i+1|k-1}}_{u_{i+1|k-1}}(u_{i|k} - u_{i+1|k-1}) \\
&\quad \cong A_{i,k}x_{i|k} + B_{i,k}u_{i|k} + E_{i,k} \\
&\qquad\qquad\qquad , i = 0, 1, \ldots, N-1
\end{aligned}
\tag{16}
$$

where,
$A_{i,k} = \nabla_x f_k(x,u)|^{x_{i+1|k-1}}_{u_{i+1|k-1}}$, $B_{i,k} = \nabla_x f_k(x,u)|^{x_{i+1|k-1}}_{u_{i+1|k-1}}$, $E_{i,k} = f_k(x_{i+1|k-1}, u_{i+1|k-1}) - A_{i,k}x_{i+1|k-1} - B_{i,k}u_{i+1|k-1}$. For multi-point linearization, it is assumed that the N-th planned input that is not calculated in the previous step is the same as the next and $(N-1)$-th planned input, i.e. $u_{N|k-1} = u_{N-1|k-1}$. Because linearization is performed using the predictions, high order linearization errors $O[(x_{i|k} - x_{i+1|k-1})^2]$and $O[(u_{i|k} - u_{i+1|k-1})^2]$ can be minimized. Using the linearized model (16), the prediction model for the state during the prediction horizon (i.e. $i \in [1, N]$) can be summarized as follows:

$$
X_k = S_x x(k) + S_u U_k + S_E, \tag{17}
$$

where,

$$
S_x = \begin{bmatrix} A_{0,k} \\ A_{1,k}A_{0,k} \\ A_{2,k}A_{1,k}A_{0,k} \\ \vdots \\ \prod_{i=0}^{N-1} A_{i,k} \end{bmatrix},
$$

$$
S_u = \begin{bmatrix} B_{0,k} & 0 & \ldots & 0 \\ A_{1,k}B_{0,k} & B_{1,k} & \ldots & 0 \\ A_{2,k}A_{1,k}B_{0,k} & A_{2,k}B_{1,k} & \ldots & 0 \\ \vdots & \vdots & \ddots & \vdots \\ \prod_{i=1}^{N-1} A_{i,k}B_{0,k} & \prod_{i=2}^{N-1} A_{i,k}B_{1,k} & \ldots & B_{N-1,k} \end{bmatrix},
$$

$$
S_E = \begin{bmatrix} I & 0 & \ldots & 0 \\ A_{1,k} & I & \ldots & 0 \\ A_{2,k}A_{1,k} & A_{2,k} & \ldots & 0 \\ \vdots & \vdots & \ddots & \vdots \\ \prod_{i=1}^{N-1} A_{i,k} & \prod_{i=2}^{N-1} A_{i,k} & \ldots & I \end{bmatrix}.
$$

Through Equation (17), the states during the prediction horizon can be predicted from the current states $x(k)$ and U_k.

1) Prediction Model Comparison: To verify the performance of the predictive model (17), a simulation was performed on the double lane change scenario with braking shown in Fig.4. Performances of prediction models against nonlinearities were compared. The simulation was conducted offline through Carsim, a high-order nonlinear vehicle simulator. The future state was predicted through actual future vehicle inputs. The states predicted by the proposed method and those predicted by existing methods were compared with the actual future behavior of the vehicle. The sampling time was set to 0.1 seconds. The states were predicted for a horizon of 20 steps, and visualized for the initial states at an interval of 10 steps.

The results are shown in Fig.5. The predictions of speed and station was omitted because the difference in accuracy was insignificant. For other states, predictions based on the single-point linearized model and predictions based on the linear bicycle model deviated significantly from actual vehicle behavior due to lack of consideration of nonlinearity. The LTV linear model [22] effectively represented nonlinearity in many areas due to multi-point linearization. However, for some of the horizons where the input was changing, the predictions diverges. On the other hand, it can be seen that the results of the nonlinear model and the proposed multi-point linearization model predict the future behavior well within a small error range. Compared with the actual future behavior of the vehicle, the error increases for predictions in the distant future due to uncertainty of the nonlinear model. However, considering that the nonlinear model-based prediction and the proposed model-based prediction are very similar, it can be confirmed that the linearization error is greatly reduced. Therefore, the proposed linearization method enables linear calculation without significantly impairing the performance of the nonlinear prediction model.

B. Model Predictive Controller Design

In this section, the design of a model prediction controller using a multi-point prediction model (17) is introduced. The cost functions and constraints to achieve the control objectives

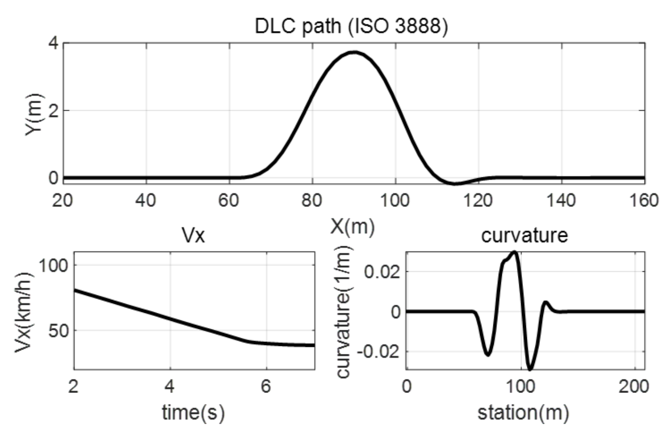

Fig. 4. Model comparison scenario

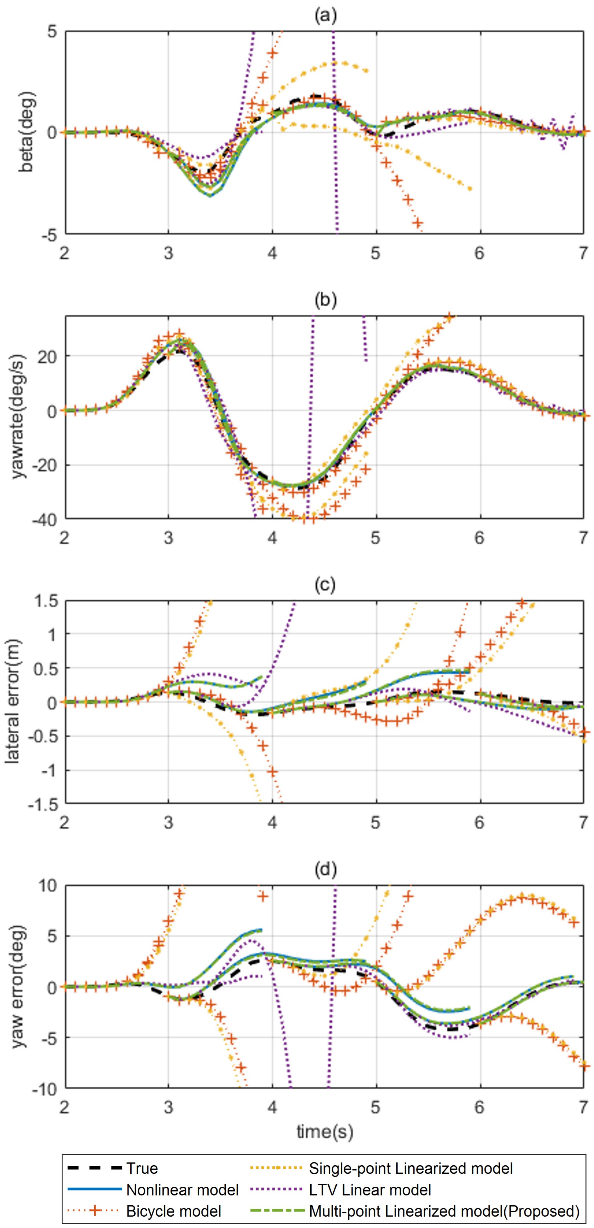

Fig. 5. Prediction model comparison results

are defined. In addition, these are transformed into quadratic optimization.

1) Cost Function: The cost function for optimization for the finite horizon of the model prediction controller is as follows.

$$\begin{aligned} J &= \sum_{i=0}^{N-1} q_{e_y}(e_{y,i+1|k})^2 + q_{e_\psi}(e_{\psi,i+1|k})^2 \\ &\quad + \Delta u_{i|k}^T \bar{R} \Delta u_{i|k} \\ &= \sum_{i=0}^{N-1} x_{i+1|k}^T \bar{Q} x_{i+1|k} + \Delta u_{i|k}^T \bar{R} \Delta u_{i|k}, \end{aligned} \tag{18}$$

where,

$$\bar{Q} = \mathrm{diag}(0,0,0,0,q_{e_y},q_{e_\psi}), \bar{R} = \mathrm{diag}(r_\delta, r_{a_x}),$$

$$\Delta u_{i|k} = \begin{cases} u_{i|k} - u(k-1) & \text{if, } \ i = 0 \\ u_{i|k} - u_{i-1|k} & \text{if, } \ i = 1,2,\ldots,N-1, \end{cases}$$

q_{e_y}, q_{e_ψ}, r_δ, and r_{a_x} are positive gains for suppressing each state and the amount of change in each input. An input sequence that minimizes the cost function has two main purposes. The first is to minimize the path tracking error, expressed by the lateral position error e_y and the heading angle error e_ψ. With this, the input sequence is generated so that the vehicle follows the path as far as possible. The second purpose is to reduce vehicle jerks, which degrade driver comfort and vehicle stability. Sudden changes in acceleration and steering angle, which are inputs of the proposed controller, can cause longitudinal and lateral jerks of the vehicle. Therefore, a cost function(18) taking this into account is used to suppress sudden changes of input. Changes of input are expressed in compact matrix form, as follows:

$$\Delta U_k = \begin{bmatrix} \Delta u_{0|k} \\ \Delta u_{1|k} \\ \vdots \\ \Delta u_{N-1|k} \end{bmatrix} = D_u U_k - U_{p,k}, \tag{19}$$

where,

$$D_u = \begin{bmatrix} 1 & 0 & \ldots & 0 \\ -1 & 1 & \ldots & 0 \\ \vdots & \vdots & \ddots & \vdots \\ 0 & 0 & \ldots & 1 \end{bmatrix}, U_{p,k} = \begin{bmatrix} u(k-1) \\ 0 \\ \vdots \\ 0 \end{bmatrix}.$$

The cost function (18) can be summarized as follows.

$$J = X_k^T Q X_k + \Delta U_k^T R \Delta U_k \tag{20}$$

where,

$$Q = \mathrm{diag}(\bar{Q}, \bar{Q}, \ldots, \bar{Q}), R = \mathrm{diag}(\bar{R}, \bar{R}, \ldots, \bar{R}).$$

Substituting the prediction model (17) and the input variation vector (19) into (18) gives the following equation.

$$\begin{aligned} J =& X_k^T Q X_k + \Delta U_k^T R \Delta U_k \\ =& (S_x x(k) + S_u U_k + S_E)^T Q (S_x x(k) + S_u U_k + S_E) \\ & + (D_u U_k - U_{p,k})^T R (D_u U_k - U_{p,k}) \\ =& (S_x x(k) + S_E)^T Q (S_x x(k) + S_E) + U_k^T (S_u^T Q S_u) U_k \\ & + 2(S_x x(k) + S_E)^T Q S_u U_k + U_k^T (D_u^T R D_u) U_k \\ & - (2U_{p,k}^T R D_u) U_k + U_{p,k}^T R U_{p,k}. \end{aligned} \tag{21}$$

Since the goal of optimization is to find the input that minimizes the cost function, terms not related to the input sequence are deleted and the quadratic cost function is summarized as follows.

$$\begin{aligned} J_u =& U_k^T (S_u^T Q S_u + D_u^T R D_u) U_k \\ & + 2[(S_x x(k) + S_E)^T Q S_u - U_{p,k}^T R D_u] U_k. \end{aligned} \tag{22}$$

2) Constraints: For stable path tracking control, tire forces must be generated within the limits of road friction. When the tire force of each wheel is required by the controller to be above the road surface friction limit, the tire loses friction and this causes unstable behavior. In particular, since the combined tire forces in the longitudinal and lateral directions must not exceed the road surface friction limit, not only the force in each direction but also the magnitude of the resultant force must be considered in situations in which both turning and braking input occur simultaneously. Therefore, the following constraints are defined to ensure that the sum of the longitudinal/lateral forces of each wheel during the prediction horizon does not exceed the road surface friction limit.

$$\sqrt{(F^j_{x,i|k})^2 + (F^j_{y,i|k})^2} \leq \mu F^j_{z,i|k} \tag{23}$$
$$, i = 0, 1, \dots, N-1, j = fl, fr, rl, rr.$$

In addition, to improve control robustness for uncertainties of the vehicle model, constraints have been applied more strictly than original constraints(23). During the prediction horizon, more stringent constraints for the distant future were applied through the robustness parameter $\eta(\in [0,1])$, leading to robustness against progressively increasing prediction errors.

$$\sqrt{(F^j_{x,i|k})^2 + (F^j_{y,i|k})^2} \leq \eta^{(i-1)} \mu F^j_{z,i|k}. \tag{24}$$

The tire force constraint (24) can be satisfied when the following equations of longitudinal force constraint and lateral force constraint are satisfied.

$$|F^j_{x,i|k}| \leq \eta^{(i-1)} \mu F^j_{z,i|k} \tag{25a}$$
$$|F^j_{y,i|k}| \leq \sqrt{(\eta^{(i-1)} \mu F^j_{z,i|k})^2 - {F^j_{x,i|k}}^2}. \tag{25b}$$

For the longitudinal force expressed in (5), its constraint (25a) can be converted into a simplified acceleration constraint because it is most affected by the longitudinal acceleration. To calculate the upper bound of the magnitude of the longitudinal acceleration by using the past prediction information, it is assumed that the N-th input plan of the previous step is the same as the $(N-1)$-th input plan as in the previous linearization process, i.e. $u_{N|k-1} = u_{N-1|k-1}$. The simplified acceleration constraint is as follows:

$$|a_{x,i|k}| \leq \min_j \bar{a}^j_{x,i|k}, \tag{26}$$

where,

$$\bar{a}^j_{x,i|k} = \begin{cases} \frac{1}{m}\frac{2}{\lambda}[\eta^{(i-1)}\mu F^j_{z,i+1|k-1} - F_D] & \text{if,} \quad j = fl, fr \\ \frac{1}{m}\frac{2}{(1-\lambda)}[\eta^{(i-1)}\mu F^j_{z,i+1|k-1} - F_D] & \text{if,} \quad j = rl, rr. \end{cases}$$

Lateral force constraints(25b) can be replaced with constraints of slip angle which create lateral forces. Again, the upper bound utilizes the past predicted value, as in the longitudinal constraint (26).

$$\begin{aligned} |\alpha^j_{i|k}| &\leq \bar{\alpha}^j_{i|k} \\ &= \frac{1}{C_0}\frac{1}{F^j_{z,i+1|k-1}}\sqrt{(\eta^{(i-1)}\mu F^j_{z,i+1|k-1})^2 - (F^j_{x,i+1|k-1})^2}. \end{aligned} \tag{27}$$

$\bar{\alpha}^i$ is the upper bound of the slip angle constraint; C_0 is the linear cornering stiffness. A simple calculation is possible by utilizing the linear cornering stiffness, which ignores the saturation of the lateral tire force. Since the cornering stiffness C_0 in the low-slip linear section is larger than the non-linear cornering stiffness $C_\alpha(\alpha)$, the constraint (27) is stricter than when using the non-linear cornering stiffness, as follows.

$$\begin{aligned} \bar{\alpha}^j_{i|k} &\leq \frac{1}{C_0}\frac{1}{F^j_{z,i+1|k-1}}\sqrt{(\mu F^j_{z,i+1|k-1})^2 - (F^j_{x,i+1|k-1})^2} \\ &\leq \frac{1}{C_\alpha(\alpha^j)}\frac{1}{F^j_{z,i+1|k-1}}\sqrt{(\mu F^j_{z,i+1|k-1})^2 - (F^j_{x,i+1|k-1})^2}. \end{aligned} \tag{28}$$

The tire forces used to calculate the upper limits (26), (27) are calculated using the predicted states and inputs though tire force models.

α_i has a nonlinear relationship with the states and the inputs expressed in (7). Therefore, we applied the multi-point linearized constraint in the same manner as the multi-point linearized prediction model (17). The linearized slip angle predictions are as follows.

$$\begin{aligned} \alpha^j_{i|k} =& \alpha^j(x_{i|k}, u_{i|k}) \\ \cong& \alpha^j(x_{i+1|k-1}, u_{i+1|k-1}) \\ &+ \nabla_x \alpha^j(x,u)|^{x_{i+1|k-1}}_{u_{i+1|k-1}}(x_{i|k} - x_{i+1|k-1}) \\ &+ \nabla_u \alpha^j(x,u)|^{x_{i+1|k-1}}_{u_{i+1|k-1}}(u_{i|k} - u_{i+1|k-1}) \\ =& \Gamma^j_{i,k} x_{i|k} + \Delta^j_{i,k} u_{i|k} + \Theta^j_{i,k}, \end{aligned} \tag{29}$$

where,

$$\Gamma^j_{i,k} = \nabla_x \alpha^j(x,u)|^{x_{i+1|k-1}}_{u_{i+1|k-1}}, \Delta^j_{i,k} = \nabla_u \alpha^j(x,u)|^{x_{i+1|k-1}}_{u_{i+1|k-1}},$$
$$\Theta^j_{i,k} = \alpha^j(x_{i+1|k-1}, u_{i+1|k-1}) - \Gamma^j_{i,k} x_{i+1|k-1} - \Delta^j_{i,k} u_{i+1|k-1},$$
$$i = 0, 1, \dots, N-1, j = fl, fr, rl, rr.$$

Equation (29) is expressed in vector form for the prediction horizon, as follows.

$$\Lambda_k = C_x X_k + C_u U_k + C_E, \tag{30}$$

where,

$$\Lambda_k = \begin{bmatrix} \alpha^{fl}_{0|k} \\ \alpha^{fr}_{0|k} \\ \alpha^{rl}_{0|k} \\ \vdots \\ \alpha^{rr}_{N-1|k} \end{bmatrix}, C_x = \begin{bmatrix} \Gamma^{fl}_{0,k} & 0 & \dots & 0 \\ \Gamma^{fr}_{0,k} & 0 & \dots & 0 \\ \Gamma^{rl}_{0,k} & 0 & \dots & 0 \\ \Gamma^{rr}_{0,k} & 0 & \dots & 0 \\ 0 & \Gamma^{fl}_{1,k} & \dots & 0 \\ \vdots & \vdots & \vdots & \vdots \\ 0 & 0 & \dots & \Gamma^{rr}_{N-1,k} \end{bmatrix},$$

$$C_u = \begin{bmatrix} \Delta^{fl}_{0,k} & 0 & \dots & 0 \\ \Delta^{fr}_{0,k} & 0 & \dots & 0 \\ \Delta^{rl}_{0,k} & 0 & \dots & 0 \\ \Delta^{rr}_{0,k} & 0 & \dots & 0 \\ 0 & \Delta^{fl}_{1,k} & \dots & 0 \\ \vdots & \vdots & \vdots & \vdots \\ 0 & 0 & \dots & \Delta^{rr}_{N-1,k} \end{bmatrix}, C_E = \begin{bmatrix} \Theta^{fl}_{0,k} \\ \Theta^{fr}_{0,k} \\ \Theta^{rl}_{0,k} \\ \Theta^{rr}_{0,k} \\ \Theta^{fl}_{1,k} \\ \vdots \\ \Theta^{rr}_{N-1,k} \end{bmatrix}.$$

The slip angle prediction is expressed as follows by substituting the prediction model Equation (17) into Equation (30).

$$\begin{aligned} \Lambda_k =& C_x(S_x x(k) + S_u U_k + S_E) + C_u U_k + C_E \\ =& (C_x S_u + C_u)U_k + (C_x S_x x(k) + C_x S_E + C_E), \end{aligned} \tag{31}$$

Finally, the constraint is defined as follows through equations (27) and (31).

$$\begin{aligned} &\begin{bmatrix} (C_x S_u + C_u)^T \\ -(C_x S_u + C_u)^T \end{bmatrix}^T U_k \\ &\leq \begin{bmatrix} \{\bar{\Lambda}_k - (C_x S_x x(k) + C_x S_E + C_E)\}^T \\ \{-\underline{\Lambda}_k + (C_x S_x x(k) + C_x S_E + C_E)\}^T \end{bmatrix}^T, \end{aligned} \tag{32}$$

where,

$$\bar{\Lambda}_k = \begin{bmatrix} \bar{\alpha}^{fl}_{0|k} \\ \bar{\alpha}^{fr}_{0|k} \\ \bar{\alpha}^{rl}_{0|k} \\ \vdots \\ \bar{\alpha}^{rr}_{N-1|k} \end{bmatrix}, \underline{\Lambda}_k = -\bar{\Lambda}_k.$$

3) Linear optimization problem: Finally, through multi-point linearization of the nonlinear prediction model and the constraints, nonlinear MPC defined as a nonlinear optimization problem(15) was changed into a quadratic cost function (22) and linear inequality constraints (26) and (32). Therefore, the nonlinear optimization problem (15) was changed into a quadratic optimization problem, and the optimal input sequence was calculated using quadratic programming (QP).

IV. Simulation Results

Simulations were conducted to verify the performance of the proposed controller. The simulations used Carsim, a high-order vehicle simulator; the proposed controller was designed using Matlab Simulink. A comparison was carried out between the proposed controller and existing controllers for a curved path. Also, the behavior of the proposed controller was analyzed with respect to the initial speed. To verify robustness against model parameter errors, additional errors of 10% were given to the vehicle model parameters, vehicle mass and moment yaw inertia, for all scenarios. Table I shows the parameters of the proposed controller used in the simulations. The controller has a prediction range of 2 seconds with an interval of 0.1 seconds, which is set in consideration of the amount of calculation and the prediction time required to cope with dangerous situations. These parameters can be adjusted according to the hardware performance and the required performance of the controller. In addition, each weight is roughly set according to the scale of the corresponding state, and then tuned in detail based on the control result.

TABLE I
CONTROL PARAMETERS

Parameter	Value
$T_s(s)$	0.1
N	20
q_{e_y}, q_{e_ψ}	10, 10
r_δ, r_{a_x}	30, 0.01
η	0.98

TABLE II
COMPUTATIONAL TIMES

Method	Avg comp. time (ms)	Max comp. time (ms)
Proposed LMPC	0.9	1.3
Single-point LMPC	0.6	1.3
NMPC (max iter.)	740	1800
NMPC (min iter.)	96	130

A. Comparison with Existing Control Methods

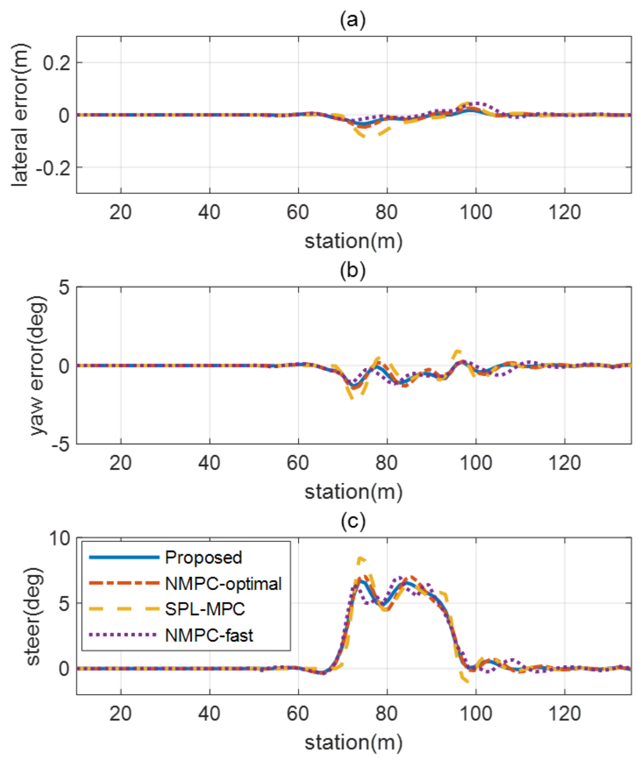

Fig. 6. Vehicle motions : Comparison of simulation results between the proposed controller and existing MPCs at low speed situation (50km/h)

The performance of the proposed LMPC was verified through comparison with NMPC and single-point linearized model-based LMPC on a curved path. The single-point linearized model-based LMPC was designed by linearizing the nonlinear model for states $x(k)$ and inputs $u(k-1)$ of each step. LMPCs was calculated using `quadprog` in matlab, and the optimality tolerance was set to 10^{-3}. This tolerance represents the degree of convergence of optimization, and the scale is set in the range in which the proposed controller converges stably. NMPC was implemented through

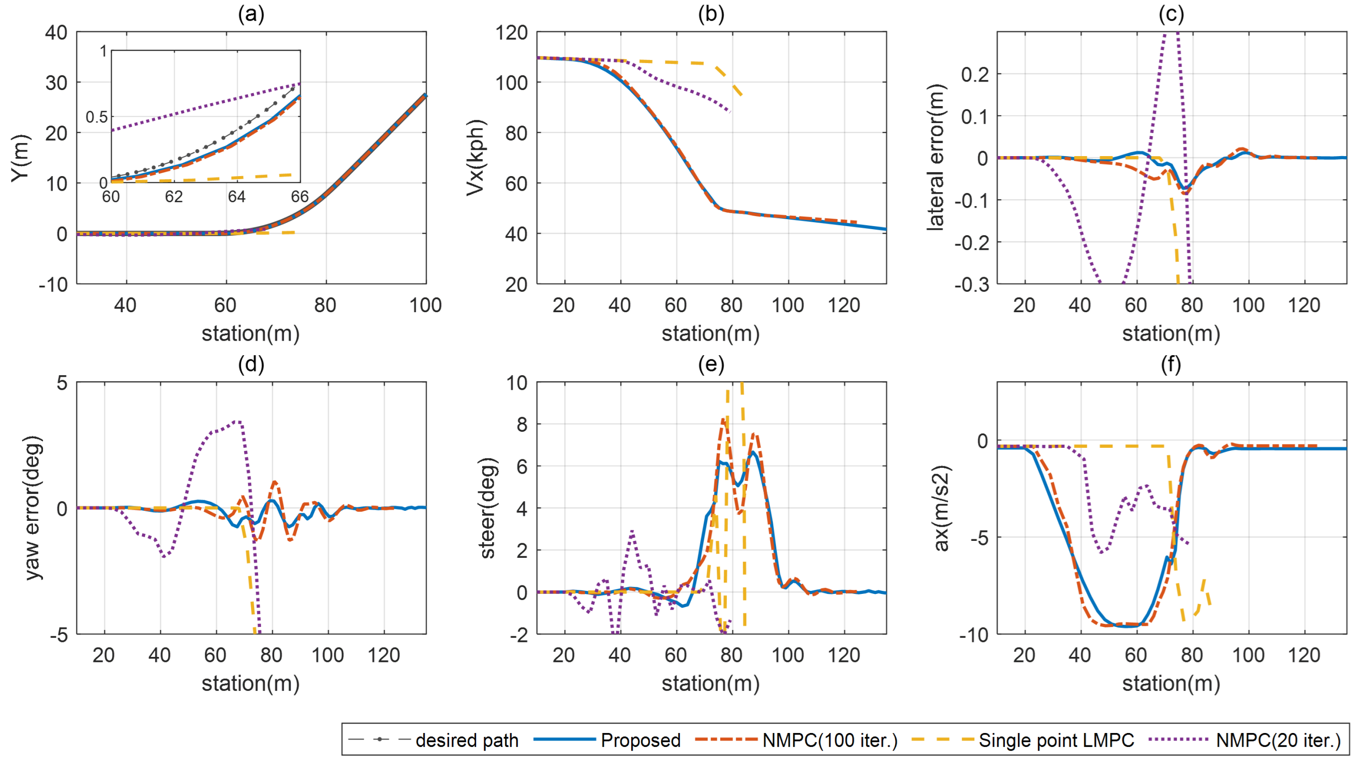

Fig. 7. Vehicle motions : Comparison of simulation results between the proposed controller and existing MPCs at high speed situation (110km/h)

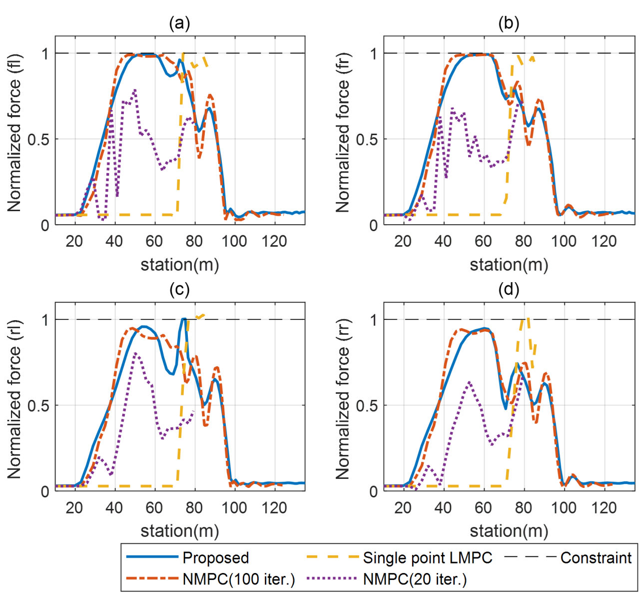

Fig. 8. Normalized resultant force of each wheel : Comparison of simulation results between the proposed controller and existing MPCs at high speed situation (110km/h)

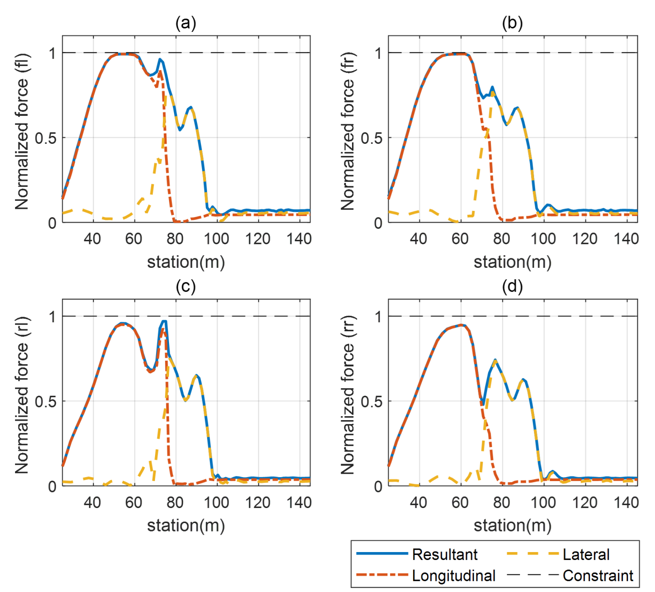

Fig. 9. Normalized forces of each wheel : Simulation result of the proposed controller at high speed situation (110km/h)

nonlinear optimization via sequential quadratic programming (SQP). SQP is a non-linear optimization method that iterates linearization and optimization by solving sub-QP problems [24], [34]. SQP was calculated using `fmincon` in matlab. For comparison of control performance and computational burden, NMPCs with sufficient iterations(< 100) and fewer than sufficient iterations (< 20) to reduce computational amount were used. Also, the optimality tolerance was set equal to the LMPC.

Fig.6 shows the control results for a low constant speed situation in which stable driving is possible without braking; Fig.7 shows the control results for a high speed turning situation that

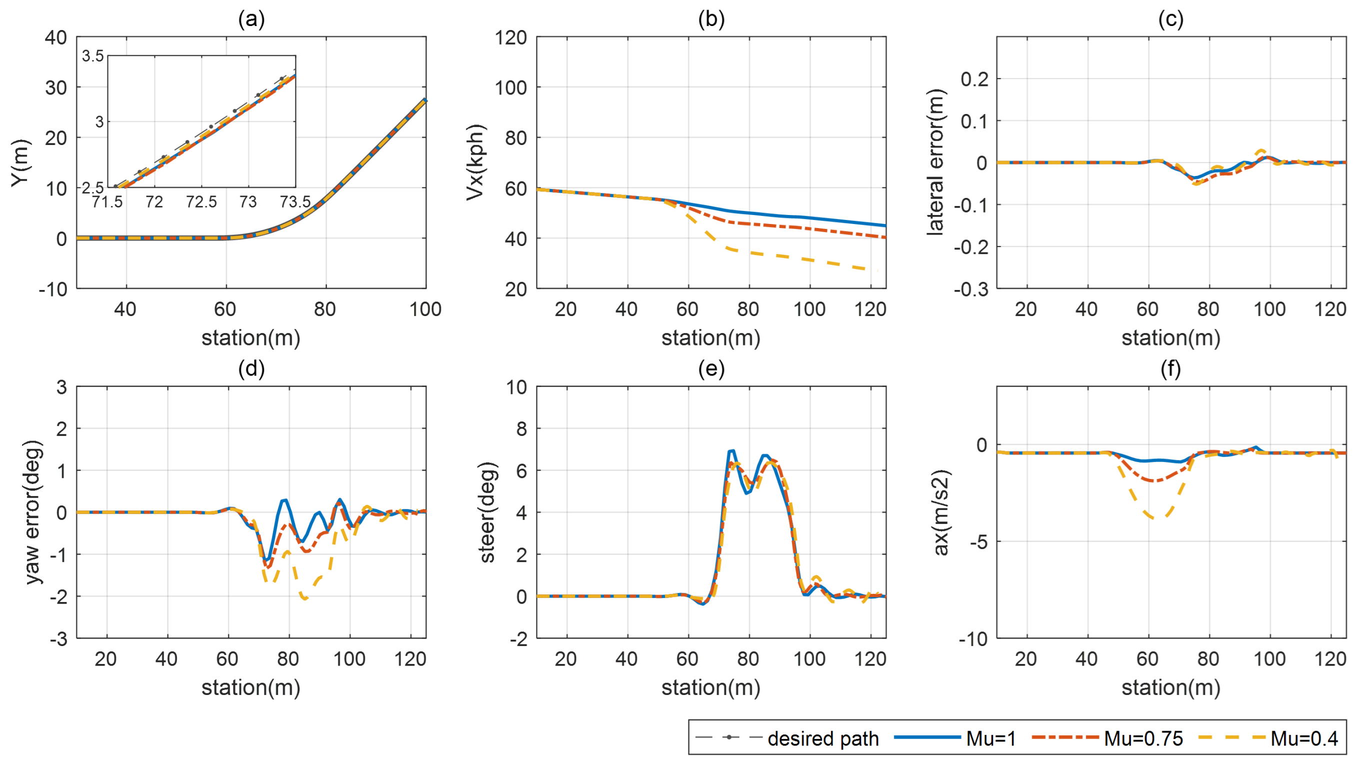

Fig. 10. Vehicle motions : Comparison of simulation results according to road conditions

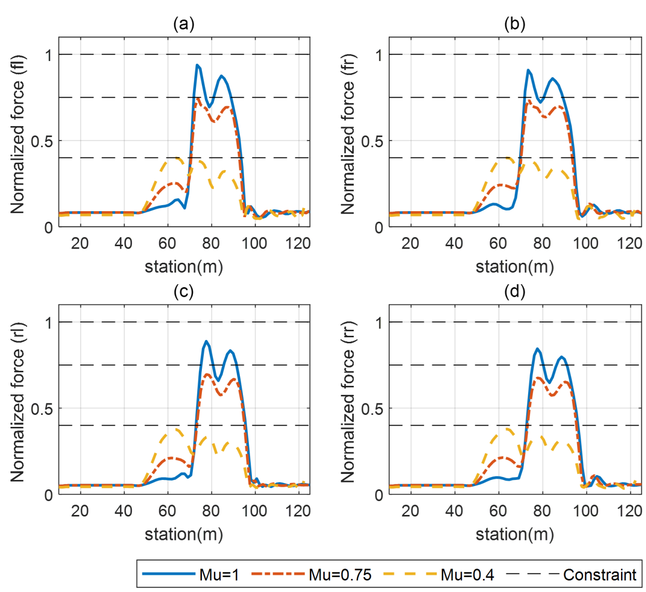

Fig. 11. Normalized resultant force of each wheel : Comparison of simulation results according to road conditions

must be accompanied by braking control. In a stable driving situation at low constant speed, the motion of the vehicle does not have much non-linearity. Therefore, all controllers including the proposed controller performed path tracking stably and accurately. However, nonlinearity of vehicle motion is maximized for the high-speed turning situation shown in Fig.7. As a result, the control performance was significantly different depending on the nonlinear prediction performance of each controller.

The single-point linearized model-based controller and NMPC with fewer iterations failed to track the path due to large linearization errors and insufficient number of iterations. These controllers did not brake in advance, and the simulation was terminated because no solution was found that satisfies the constraints during turning. Conversely, the proposed controller and NMPC, with sufficient iterations, achieved stable and accurate control results because of their accurate prediction models. These controllers showed stable control results in that the normalized resultant force of each tire, as shown in Fig.8, did not exceed the road friction limit, i.e. $\sqrt{(F_x)^2 + (F_y)^2}/F_z < \mu$. Also because the system performed accurate steering control, the path tracking errors shown in Fig.7(c) and Fig.7(d) were within 0.1m of the lateral error and 2° of the heading error for both controllers. For stable control, the proposed controller suppresses the generation of lateral tire force during turning through appropriate braking prior to steering. This braking control was performed despite the fact that there was no command related to the longitudinal behavior other than the constraints on the tire force on each wheel. The normalized tire forces for each direction shown in Fig.9 not only control the vehicle so that the force in each direction does not exceed the road friction limit, but also ensure that the resultant force does not exceed the road friction limit at moments when forces in both directions occur simultaneously.

Table II shows the calculation time consumed by each controller in the high-speed turning situation. For LMPCs, a maximum of 6 iterations occurred to satisfy the optimality tolerance. Compared to NMPC, calculation through LMPC has a large difference in calculation speed because not only the number of iterations is small, but also there is a difference in the amount of calculation during one iteration. Nevertheless, the proposed controller has a level of control performance equivalent to that of the nonlinear controller.

Through comparison with existing controllers, it was verified that the proposed controller has the nonlinear processing capability of the NMPC and, at the same time, exhibits breakthrough computational efficiency by implementing LMPC through multi-point linearization.

B. Comparison of Behavior Changes According to Changes in Road Conditions

Since the purpose of this study was to prevent individual tire forces from exceeding the road friction limit, control performance for various road surface conditions was verified. Simulation were conducted with the same approach speed for a total of three road surfaces, from a road surface with a large friction limit to a slippery road surface. Vehicle behavior resulting from control and forces exerted on each tire are shown in Fig.10 and Fig.11, respectively. As a result of the control, the road surface limit condition was satisfied, as shown in Fig. 11, on all three road surfaces. In addition, our controller showed accurate path tracking performance through stable tire force generation and proper steering control. At a road friction limit of 1, there was little braking control because system was able to generate sufficient lateral forces. However, as the road surface became slippery, the speed was reduced to secure stability during turning. In particular, on the slippery road surface, a braking force close to the road friction limit was applied to actively prepare for future behavior. Through this, it can be confirmed that the proposed controller performs appropriate control according to road surface limitations without unnecessary braking.

V. CONCLUSION

In this study, we propose an MPC using a multi-point linearized model for stable and accurate path tracking. Compared to the existing single-point based linearization method, the newly proposed multi-point linearization method dramatically reduces the linearization error. Using the proposed controller, non-linear vehicle behavior is accurately handled through efficient calculations. Utilizing this method, the proposed controller accurately predicts vehicle behavior and ensures that tire force of each wheel, expressed in a non-linear manner, do not exceed road friction limit. In situations in which unstable lateral motion is expected due to high speed or slippery road surfaces, vehicle stability is guaranteed through braking input generated by constraints on tire forces. The improved computational efficiency and control performance of the proposed controller for the nonlinear vehicle model were verified through simulation results and a comparison with other control methods. In addition, results for various road surface conditions showed that stable and accurate path tracking performance could be obtained through optimal braking and steering input that satisfied the road friction limits.

ACKNOWLEDGEMENT

This research was partly supported by the BK21 FOUR Program of the National Research Foundation Korea (NRF) grant funded by the Ministry of Education (MOE), the Technology Innovation Program (20014983, Development of autonomous chassis platform for a modular vehicle) funded By the Ministry of Trade, Industry Energy (MOTIE, Korea), the National Research Foundation of Korea (NRF) grant funded by the Korea government (MSIP) (No. 2020R1A2B5B01001531), and the grant (21TLRP-C152499-03) from Transportation Logistics Research Program funded by Ministry of Land, Infrastructure and Transport (MOLIT) of Korea government and Korea Agency for Infrastructure Technology Advancement (KAIA).

REFERENCES

[1] David Gerónimo, Antonio M. López, Angel D. Sappa, and Thorsten Graf. Survey of pedestrian detection for advanced driver assistance systems. *IEEE Transactions on Pattern Analysis and Machine Intelligence*, 32(7):1239–1258, 2010.

[2] Olaf Gietelink, Jeroen Ploeg, Bart De Schutter, and Michel Verhaegen. Development of advanced driver assistance systems with vehicle hardware-in-the-loop simulations. *Vehicle System Dynamics*, 44(7):569–590, 2006.

[3] Yunhyoung Hwang and Seibum B. Choi. Adaptive Collision Avoidance Using Road Friction Information. *IEEE Transactions on Intelligent Transportation Systems*, 20(1):348–361, 2019.

[4] J. Piao and M. McDonald. Advanced driver assistance systems from autonomous to cooperative approach. *Transport Reviews*, 28(5):659–684, 2008.

[5] Chang Wang, Qinyu Sun, Yingshi Guo, Rui Fu, and Wei Yuan. Improving the User Acceptability of Advanced Driver Assistance Systems Based on Different Driving Styles: A Case Study of Lane Change Warning Systems. *IEEE Transactions on Intelligent Transportation Systems*, 21(10):4196–4208, 2020.

[6] W. Lim, S. Lee, M. Sunwoo, and K. Jo. Hierarchical trajectory planning of an autonomous car based on the integration of a sampling and an optimization method. *IEEE Transactions on Intelligent Transportation Systems*, 19(2):613–626, 2018.

[7] Jie Ji, Amir Khajepour, Wael William Melek, and Yanjun Huang. Path planning and tracking for vehicle collision avoidance based on model predictive control with multiconstraints. *IEEE Transactions on Vehicular Technology*, 66(2):952–964, 2017.

[8] Claudiu Pozna, Fritz Troester, Radu Emil Precup, József K. Tar, and Stefan Preitl. On the design of an obstacle avoiding trajectory: Method and simulation. *Mathematics and Computers in Simulation*, 79(7):2211–2226, 2009.

[9] Xuemin Hu, Long Chen, Bo Tang, Dongpu Cao, and Haibo He. Dynamic path planning for autonomous driving on various roads with avoidance of static and moving obstacles. *Mechanical Systems and Signal Processing*, 100:482–500, 2018.

[10] Chongfeng Wei, Richard Romano, Natasha Merat, Y. Wang, C. Hu, H. Taghavifar, Foroogh Hajiseyedjavadi, and Erwin R. Boer. Risk-based autonomous vehicle motion control with considering human driver's behaviour. *Transportation Research Part C: Emerging Technologies*, 107(September 2018):1–14, 2019.

[11] Moveh Samuel, Mohamed Hussein, and Maziah Binti. A Review of some Pure-Pursuit based Path Tracking Techniques for Control of Autonomous Vehicle. *International Journal of Computer Applications*, 135(1):35–38, 2016.

[12] Hyung Gyu Park, Kyoung Kwan Ahn, Myeong Kwan Park, and Seok Hee Lee. Study on Robust Lateral Controller for Differential GPS-Based Autonomous Vehicles. *International Journal of Precision Engineering and Manufacturing*, 19(3):367–376, 2018.

[13] Gerasimos Rigatos and Pierluigi Siano. An H-infinity feedback control approach to autonomous robot navigation. *IECON Proceedings (Industrial Electronics Conference)*, pages 2689–2694, 2014.

[14] Muhammad Aizzat Zakaria, Hairi Zamzuri, Rosbi Mamat, Saiful Amri Mazlan, Mohd Azizi Abd Rahman, and Abdul Hadi Abd Rahman. Dynamic curvature path tracking control for autonomous vehicle: Experimental results. *2014 International Conference on Connected Vehicles and Expo, ICCVE 2014 - Proceedings*, pages 264–269, 2014.

[15] Brian Paden, Michal Čáp, Sze Zheng Yong, Dmitry Yershov, and Emilio Frazzoli. A survey of motion planning and control techniques for self-driving urban vehicles. *IEEE Transactions on Intelligent Vehicles*, 1(1):33–55, 2016.
[16] Shaobing Xu and Huei Peng. Design, Analysis, and Experiments of Preview Path Tracking Control for Autonomous Vehicles. *IEEE Transactions on Intelligent Transportation Systems*, 21(1):48–58, 2020.
[17] Jiechao Liu, Paramsothy Jayakumar, Jeffrey L. Stein, and Tulga Ersal. A nonlinear model predictive control formulation for obstacle avoidance in high-speed autonomous ground vehicles in unstructured environments. *Vehicle System Dynamics*, 56(6):853–882, 2018.
[18] John Wurts, Jeffrey L. Stein, and Tulga Ersal. Collision Imminent Steering at High Speeds on Curved Roads Using One-Level Nonlinear Model Predictive Control. *IEEE Access*, 9(8):39292–39302, 2021.
[19] Huarong Zheng, Rudy R Negenborn, and Gabriel Lodewijks. Trajectory tracking of autonomous vessels using model predictive control. *IFAC Proceedings Volumes*, 47(3):8812–8818, 2014.
[20] Efstathios Siampis, Efstathios Velenis, and Stefano Longo. Predictive rear wheel torque vectoring control with terminal understeer mitigation using nonlinear estimation. *Proceedings of the IEEE Conference on Decision and Control*, 54rd IEEE(Cdc):4302–4307, 2015.
[21] Efstathios Siampis, Efstathios Velenis, and Stefano Longo. Rear wheel torque vectoring model predictive control with velocity regulation for electric vehicles. *Vehicle System Dynamics*, 53(11):1555–1579, 2015.
[22] Paolo Falcone, Francesco Borrelli, Jahan Asgari, Hongtei Eric Tseng, and Davor Hrovat. Predictive active steering control for autonomous vehicle systems. *IEEE Transactions on control systems technology*, 15(3):566–580, 2007.
[23] Matthew Brown, Joseph Funke, Stephen Erlien, and J. Christian Gerdes. Safe driving envelopes for path tracking in autonomous vehicles. *Control Engineering Practice*, 61:307–316, 2017.
[24] Qifan Tan, Penglei Dai, Zhihao Zhang, and Jay Katupitiya. MPC and PSO based control methodology for path tracking of 4WS4WD vehicles. *Applied Sciences (Switzerland)*, 8(6):1–24, 2018.
[25] Eugenio Alcalá, Vicenç Puig, and Joseba Quevedo. LPV-MPC Control for Autonomous Vehicles. *IFAC-PapersOnLine*, 52(28):106–113, 2019.
[26] Janick V. Frasch, Andrew Gray, Mario Zanon, Hans Joachim Ferreau, Sebastian Sager, Francesco Borrelli, and Moritz Diehl. An auto-generated nonlinear MPC algorithm for real-time obstacle avoidance of ground vehicles. *2013 European Control Conference, ECC 2013*, pages 4136–4141, 2013.
[27] Lars Grüne and Jürgen Pannek. Nonlinear model predictive control. In *Nonlinear model predictive control*, pages 45–69. Springer, 2017.
[28] R. Findeisen and F. Allgower. An introduction to non-linear model predictive control. *Control . 21st Benelux Meeting on Systems and Control, Veidhoven.*, 11:1–23, 2002.
[29] Eunjae Lee, Hojin Jung, and Seibum Choi. Tire lateral force estimation using kalman filter. *International Journal of Automotive Technology*, 19(4):669–676, Aug 2018.
[30] M. Doumiati, A. C. Victorino, A. Charara, and D. Lechner. Onboard real-time estimation of vehicle lateral tire–road forces and sideslip angle. *IEEE/ASME Transactions on Mechatronics*, 16(4):601–614, 2011.
[31] Kyoungseok Han, Eunjae Lee, Mooryong Choi, and Seibum B. Choi. Adaptive Scheme for the Real-Time Estimation of Tire-Road Friction Coefficient and Vehicle Velocity. *IEEE/ASME Transactions on Mechatronics*, 22(4):1508–1518, 2017.
[32] Jacob Svendenius and Magnus Gäfvert. A brush-model based semi-empirical tire-model for combined slips. *SAE Technical Papers*, 2004(724), 2004.
[33] Magnus Gafvert and Jacob Svendenius. Construction of Novel Semi-Empirical Tire Models for Combined Braking and Cornering. (April):2–67, 2003.
[34] Qilun Zhu, Simona Onori, and Robert Prucka. Nonlinear economic Model Predictive Control for SI engines based on Sequential Quadratic Programming. *Proceedings of the American Control Conference*, 2016-July:1802–1807, 2016.

Jonghyup Lee received the B.S. degree in mechanical engineering from Korea Advanced Institute of Science and Technology (KAIST), Deajeon, Korea, and M.S. in Mechanical Engineering from the Korea Advanced Institute of Science and Technology(KAIST), in 2015 and 2017, respectively. Since 2019, he is currently pursuing the Ph.D. degree in Mechanical engineering at KAIST. His current research interests include vehicle safety systems, vehicle dynamics and control, and intelligent tires.

Seibum.B.Choi received B.S. degree in mechanical engineering from Seoul National University, Korea, M.S. degree in mechanical engineering from Korea Advanced Institute of Science and Technology (KAIST), Korea, and the Ph.D. degree in controls from the University of California, Berkeley in 1993. Since 2006, he has been with the faculty of the Mechanical Engineering department at KAIST. His research interests include fuel saving technology, vehicle dynamics and control, and application of self-energizing mechanism.